Mine Water and the Environment (2022) 41:1040–1054
https://doi.org/10.1007/s10230-022-00905-3

TECHNICAL ARTICLE

Ochre Particles in River Sediments in Coal Mining Areas (A Study of the Kizel Coal Basin, Russia)

Elena Menshikova[1] · Boris Osovetsky[1] · Sergey Blinov[1] · Pavel Belkin[1] · Elena Tomilina[1] · Irina Badyanova[1]

Received: 30 September 2021 / Accepted: 30 October 2022 / Published online: 16 November 2022

Abstract

Ochre particles in modern alluvium were studied in the area affected by the development of the Kizel coal basin deposits (Perm Krai, Russia) to establish their material composition. The purpose of this study was to determine the characteristics of the morphology and material composition of ochre particles, as well as their role as concentrators and mobilizers of toxic metals in river systems. Using scanning electron microscopy, microprobe analysis, inductively coupled plasma mass spectrometry, and x-ray diffraction analysis, we found a wide range of ochre particle types, micro- and nano-textures, and material compositions. Toxic elements found in the ochre particles include (in wt.%): Cu (up to 2.56), Zn (up to 2.04), Co (up to 0.29), Sb (up to 0.23), Hg (up to 0.13), and As (up to 0.10).

The diffraction data revealed that an important portion of the substance in the ochre composition is cryptocrystalline. Terrigenous components (quartz, feldspars, plagioclases, clay minerals, hematite) and authigenic components (goethite, carbonates) dominate the composition of the crystalline part of the ochre. Ochres in this area are the main toxic element concentrators; they actively migrate in the aquatic environment over long distances and deserve special attention in environmental monitoring studies.

Keywords Mineral composition · Microtexture · Nanotexture · Toxic elements · Environmental monitoring

Introduction

Ochres are widespread on the Earth's surface. They compose the upper horizons of weathered nickel-bearing rocks, are products of brown iron deposits, and represent the main material of many other supergene environments (Butt and Cluzel 2013; Harraz 2013; König 2021).

Ochre is a mineral-concentrator of toxic elements in many areas of the world with a high technogenic impact (Acharya and Kharel 2020; Campaner et al. 2014; Torre et al. 2019; Zakrutkin et al. 2020). Because of their unique material composition and porous structure, ochres aggregates have high sorption properties (Copaja et al. 2020; Dauvalter 2012; Erguler and Erguler 2015).

Areas of coal deposit development and the areas adjacent to them can be contaminated with potentially toxic elements. One specific example is the territory of the Kizel coal basin (Perm Krai, Russia). Coal mining began here in the eighteenth century and was halted in 2002. Widespread contamination of areas associated with coal mining has been observed in large areas, including the areas surrounding the cities of Gubakha, Kizel, and Aleksandrovsk.

The formation of ochreous sediments in this area is primarily due to the specific composition of the rocks of the Kizel coal basin's coal-bearing formation. Sandstones, siltstones, argillites, and shales with limestone interbeds

✉ Pavel Belkin
pashabelkin@mail.ru

Elena Menshikova
menshikova_e@list.ru

Boris Osovetsky
opal@psu.ru

Sergey Blinov
blinov_s@mail.ru

Elena Tomilina
tomilinaelena.psu@yandex.ru

Irina Badyanova
kataev7@psu.ru

[1] Department of Geology, Perm State University, Bukireva St. 15, Perm 614990, Russia

comprise the coal-bearing stratum (Visean stage of the Lower Carboniferous). The rocks of the coal-bearing stratum contain finely dispersed pyrite and organic sulphur, with sulphide and organic sulphur content reaching 12–15%. As a result, sulphur is one of the primary active elements in the coal-bearing stratum, determining the acid–base and redox conditions for sediment accumulation. The processes of element concentration on the hydrogen sulphide geochemical barrier, their leaching in the oxidation zone, and the formation of products that affect the ecological state of the territory are actively developing (Maximovich and Khayrulina 2014; Menshikova et al. 2020; Pyankov et al. 2021).

The oxidation of sulphide minerals, which results in the formation of acidic waters containing high concentrations of metals and metalloids, is regarded as one of the most serious environmental consequences of mining and has become quite common around the world. These issues have received a lot of attention in major synthesis studies on mining waste (Lottermoser 2007), scientific reviews, mine drainage publications (Espana 2007; Kefeni et al. 2017; Wei et al. 2016, 2017), and guidelines of the International Network for Acid Prevention (INAP 2021).

The cessation of mining operations and the flooding of mines in the Kizel coal basin did not stop the environmental problems. The main sources of pollution in the area are the discharge of acid mine water and surface runoff from rock dumps and industrial sites (Imaikin 2014; Maximovich and Khayrulina 2014), but today, some rivers that receive mine water are even more polluted than they were during the coal mining period. According to research (Dvinskikh et al. 2015), the current influx of iron compounds into the Kama Reservoir from the watersheds of the Yaiva and Kosva Rivers exceeds the discharge during the active coal mining period. The scope of this process is demonstrated by the analysis of long-term series of satellite imagery of this territory (Berezina et al. 2018; Pyankov et al. 2021). Large volumes of ochreous sediments were formed here due to the inflow of mine water.

Iron hydroxide migrates in river waters in a variety of forms. Flaky iron hydroxide particles are one form; most are less than 0.1 mm in size and migrate in suspension. Because of the flotation characteristic of highly flattened low-density particles, their migration capacity is exceptional. An important portion of them become colloidal solution components (micelles). The most active migration processes in the study area occur during floods (Lyubimova et al. 2016). As confirmed by studies on the territory in southeastern Ireland (Herr and Gray 1996), hydrological factors, along with pH, are the most important factors in the accumulation of potentially toxic metals in such river systems.

The geochemical role of ochre is manifested in the active sorption of small elements, among which Cu, Zn, Cd, Co, Cr, Ni, Pb, As, and Sb can be present in important amounts in areas of severe technogenic pollution associated with the active inflow of mine-influenced waters. This has been confirmed by numerous studies on various mining areas around the world, including coal regions in Pennsylvania (USA) (Cravotta 2008), copper mines in Libiola, Italy (Consani et al. 2017; Marescotti et al. 2012), coal deposits in India (Sahoo et al. 2012), deposits in the Iberian Pyrite Belt (Valente et al. 2015), sulphide mines in Finland (Kumpulainen et al. 2007), and elsewhere.

During the low-water period, ochre deposition from river suspensions occurs on floodplains and near-channel shallows. Their migration resumes the following year, during seasonal flooding. Colloidal ochre particles are deposited at certain geochemical barriers or as a result of micelle loss of positive charge when merging with other solutions that contain, for example, negatively charged silica particles. Massive colloidal ochre deposition can cause a local increase in the concentration of toxic elements in bottom sediments in some areas, including populated areas.

Numerous studies have shown that newly formed minerals are involved in cycles of "retention ↔ release" of hydrogen ions, sulphate, and a variety of metals (e.g. Espana et al. 2005; Kupka et al. 2012; Nordstrom 2011; Santisteban et al. 2016; Valente et al. 2013). Laboratory experiments with such sediments have revealed that their amorphous phases have the highest exchange potential (Carbone et al. 2013; Tarutis and Unz 1995). It has also been established that the mineral composition of ochreous sediments is affected by the pH of the medium, metal ion concentrations, and organic matter (Equeenuddin et al. 2010; Jönsson et al. 2006). Many researchers regard the integration of mineralogical methods for studying waste to be an important tool for solving complex waste management problems in the mining industry (Jamieson et al. 2015).

The Kama Reservoir is the final point of migration for the main mass of ochre particles in the study area. As part of the reservoir bottom sediments, ochre continues to function as toxic element concentrators and potential sources of secondary water pollution, particularly when the chemical parameters and dynamics of the medium of circulating solutions change.

The purpose of this research was to conduct a thorough examination of the morphologic properties and material composition of ochre particles in the area affected by the mining of the Kizel coal basin. The research objectives included: (1) determining the quantitative distribution of ochre in bottom sediments of the area's main river; (2) studying the morphology and micro- and nano-texture of ochre aggregates using scanning electron microscopy (SEM); and (3) determining the chemical and mineral composition of the ochre. A broad integration of research methods enables a comprehensive understanding of ochre aggregates as complex polymineral and polygenetic natural formations in areas

of negative technogenic impact. Moreover, it is assumed that the features of ochre particle composition can be used to solve complex environmental problems in similar areas.

Area and Objects of Research

We investigated the bottom sediments of the Kosva River (Kama River basin) on the territory of the Kizel coal basin, as well as upstream and downstream of the river (Fig. 1, Table 1). The most detailed sampling was carried out in two areas: immediately in the zone of coal-mining impact (12 sampling sites); and 50 km downstream (3 sampling sites). Sampling was also conducted (1 sampling point) at a site 20 km upstream of the Kosva River outside the zone of influence of the coal deposit. Samples up to 0.5 kg were taken from floodplain facies, riverbed shoals, and bottom sediments at the sampling points (Fig. 2). Each sample was formed from 10 point samples of bottom sediment in the study areas, which were taken with a polymeric scoop to limit the possible input of metals.

The territory of the Kosva River basin and the Kizel Coal basin is located within the West Urals folding zone. The geological structure of the territory involves sedimentary rocks of Paleozoic age (from the Lower Devonian to the Artinsky stage of the Lower Permian) with a total thickness of 3000–4000 m (Fig. 3). The eastern part of the territory, where the vast Shirokovsky reservoir is located, is composed of Upper Vendian rocks. The Vendian system in the International Stratigraphic Scale corresponds to the upper series of the Ediacaran system (Grazhdankin et al. 2009, 2015).

The lower part of the Kosva river's watershed is located within the eastern margin of the East European Plain and drains rocks of the Kungur and Ufimian stages of the

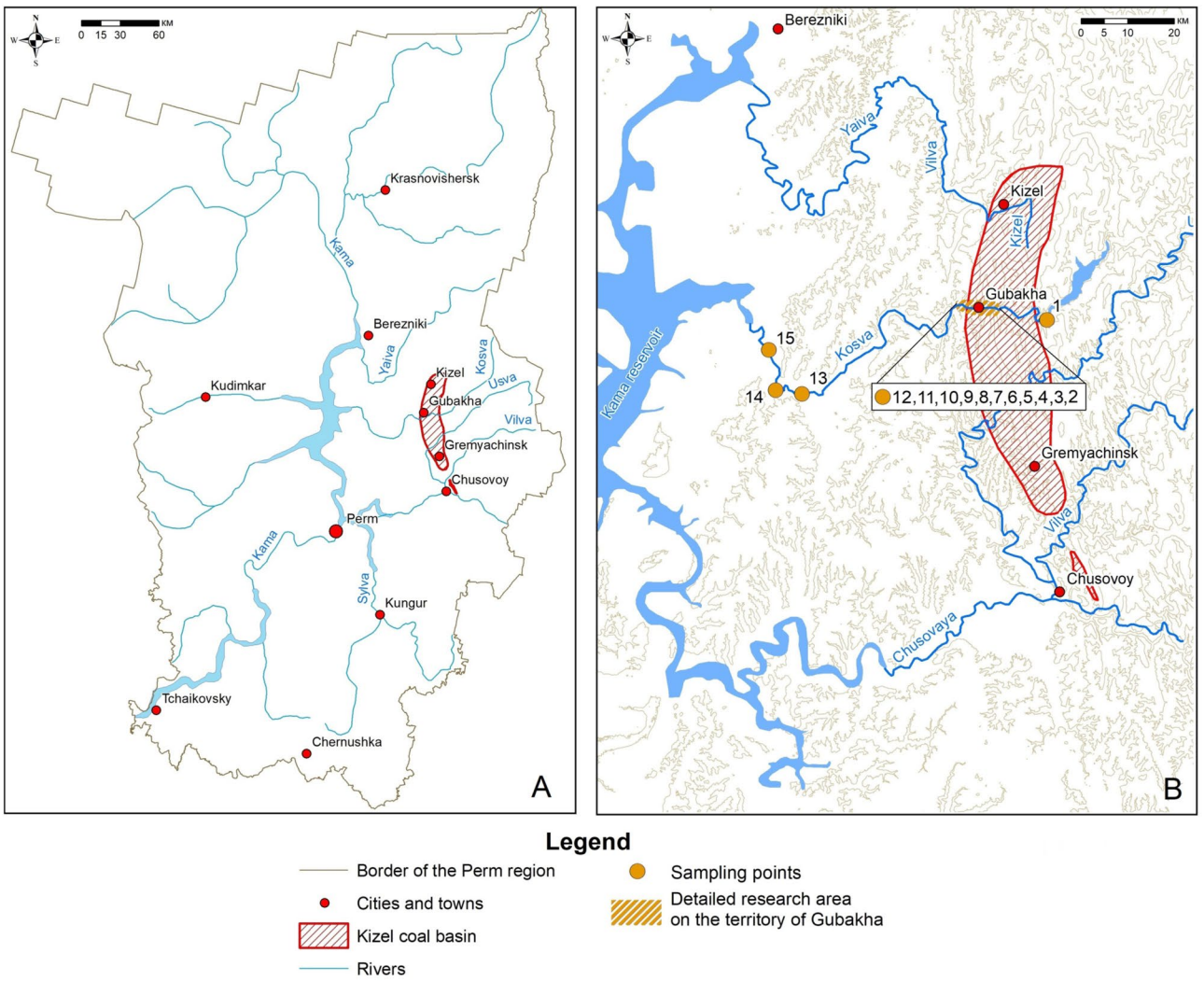

Fig. 1 Location of the study area (the Kizel Coal basin) on the map of Perm Region, Russia: **A** position of the Kizel Coal Basin in the territory of Perm Region; **B** places of sampling

Table 1 Coordinates of sampling sites from the Kosva River

Sample site	Position of sampling sites	Coordinates (WGS-84)	
		Latitude	Longitude
1	Above the impact of coal mine development	58°50′5.34″N	57°47′16.95″E
2	The area around the town of Gubakha	58°51′53.87″N	57°36′45.58″E
3		58°51′42.59″N	57°36′37.33″E
4		58°51′34.93″N	57°36′10.45″E
5		58°51′53.52″N	57°35′48.90″E
6		58°51′56.57″N	57°35′33.40″E
7		58°51′58.43″N	57°35′30.91″E
8		58°51′53.88″N	57°34′4.66″E
9		58°52′7.51″N	57°32′29.13″E
10		58°51′56.16″N	57°30′40.37″E
11		58°52′2.57″N	57°29′55.44″E
12		58°51′58.82″N	57°29′29.58″E
13	Downstream of the Kosva River	58°42′22.16″N	56°50′18.90″E
14		58°43′27.05″N	56°45′34.14″E
15		58°47′51.03″N	56°44′38.47″B

Fig. 2 Ochre sediments on the Kosva River channel bank: **A**, **B**, **C** around the town of Gubakha; **D**, **E**, **F** in the downstream of the Kosva River

Lower Permian with overlying Quaternary sediments. The Solikamsk and Sheshma horizons are part of the Ufimian Stage. Some researchers attribute the Sheshma horizon to the Kazanian Stage (corresponding to the Rhodian Stage) (Benton 2012; Lozovsky et al. 2009; Plyusnin et al. 2021), and the Solikamsk Horizon to the Kungurian (corresponding

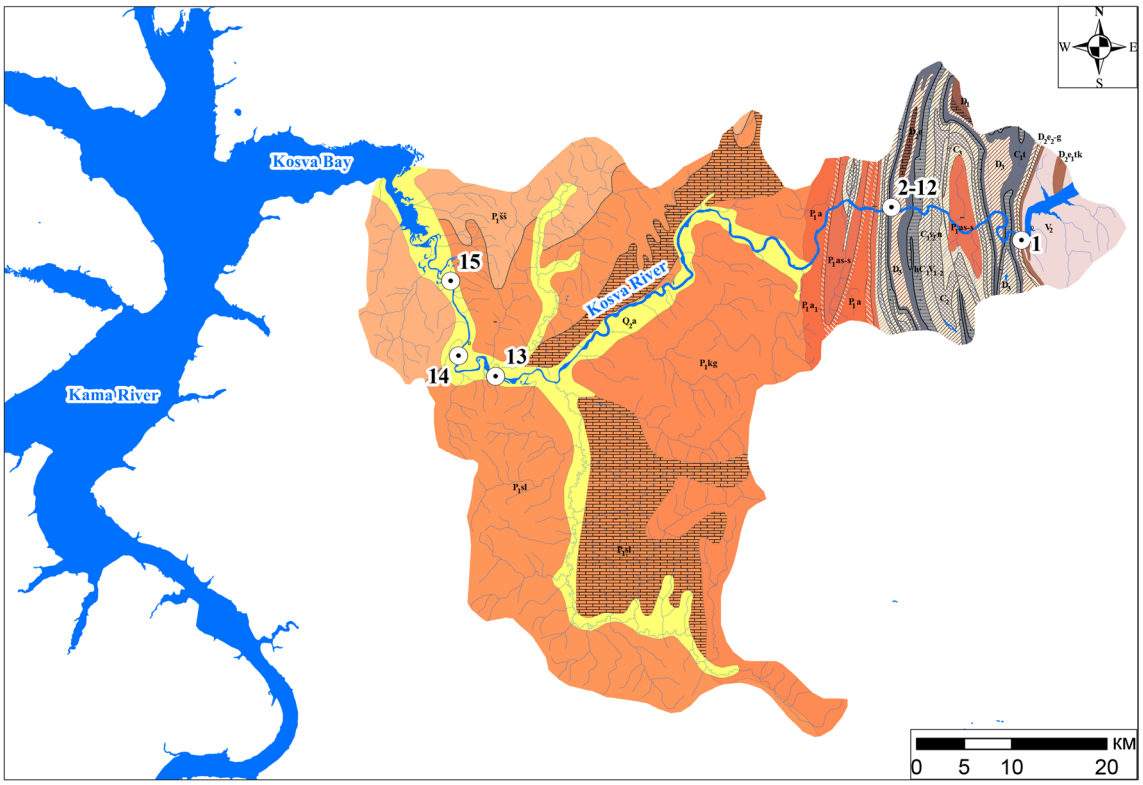

Legend

Sample location

Cenozoic

Quaternary System

Q_2a Alluvial gravel, sand, loam, sapropel clay, peat

Paleozoic

Permian System

Lower Series

P_1ušš Ufimian Stage. Sheshmian Horizon. Stage. Gypsum red-colored sandstone, mudstone, clay with lenses of clayey limestone marl and conglomerate, inclusions of malachite and azurite

P_1usl Ufimian Stage. Solikamian Horizon. Laminated marl, limestone, sandstone

P_1usl Ufimian Stage. Solikamian Horizon. Sandstone, siltstone, argillite, rarely conglomerate, limestone, marl

P_1kg Kungurian Stage. sandstone, argillite, salt (halite), gypsum, and hydrite, rarely conglomerates, dolomite

P_1a Argillite, siltstone, sandstone and conglomerate with marl and limestone interlayers

P_1a_1 Lower Artinskian Substage. Silicified limestone

P_1as-s Asselian and Samarian Stages. Foraminiferous limestone, organogenic-fragmentary, silicified in sections

Carboniferous System

Upper Series

C_3 Upper Carboniferous. Limestone, often dolomitized, dolomite

C_2 Middle Carboniferous. Limestone, dolomite, lime-clay shale, mudstone, marls at the base of conglomerate-breccia.

Lower Series

C_1v_2-s Middle and Upper Visean Substage of the Visean Stage and Serpukhovian Stage. Limestone, dolomitized limestone, and dolomite

hC_1v_1-s Visean Stage. Lower Viseian and lower part of the Middle Viseian substage. Carbonaceous sequence. Alternating quartz sandstone, siltstone, mudstone, interlayer of coal, in the upper and lower parts of the sequence rare interlayer of limestone

C_1t Tournaisian Stage. Lime-clay and siliceous-clay shale, limestone, less often sandstone, siltstone

Devonian System

Upper Series

D_3 Upper Devonian. Limestone, shale, quartz sandstone, siltstone, clays at the base

D_2e_2-g Upper Eifelian Substage of the Eifelian Stage and the Zhizhinskii Stage. Limestone, less frequently dolomite and marl

Lower Series

D_2e Limestone, rarely dolomite, quartz sandstone, rarely clay shale

D_2e_1-tk Lower Eifelian Stage. Takatinskaya Substage. Quartz sandstone with interlayer of clay shale, conglomerate at the base

D_1 Lower Devonian. Interbedded quartz sandstone, siltstone, clay and sandy shale

Proterozoic

Vendian System

V_2 Lower Vend. Sylvitskaya Stage. Interbedded quartz sandstone, siltstone, clay shale

Fig. 3 Geological map of the study area (the basin of the Kosva River) with the location of sampling points

to the Leonardian Stage) (Kotlyar 2015; Lucas and Shen 2016). Also, some researchers believe the Ufimian Stage should be the middle division of the Permian system (Plusnin et al. 2021). The above-described allocation of the tiers and horizons according to the general stratigraphic (geochronological) scale are in accordance with the Russian Stratigraphic Code 2019 and the Resolutions of the International Stratigraphic Committee 2012, 2013, and 2016.

Methods

Laboratory sample processing and analytical studies were carried out at the Centre for Collective Use of Perm State University. Representative samples were taken, weighed, ground to less than 1.0 mm approximately, dried in a drying box, and sifted into size classes (mm): more than 1; 1–0.5; 0.5–0.25; 0.25–0.1; 0.1–0.05 and less than 0.05. After weighing, each class of particles was examined under a NIKON SMZ 745 binocular microscope (Nikon, Tokyo, Japan) to evaluate the mineral composition and determine the proportion of ochre types.

Qualitative mineralogical analysis showed that the studied sediments contain grains of quartz, feldspars, mica, magnetite, hematite, chromite, pyroxenes, epidote, and ochre particles. The quantitative content of ochres in each class was estimated from a representative sample of 500 grains.

Then, monofractions of the ochre particles were selected from seven samples to determine the concentrations of trace elements. The concentrations of trace elements in the ochre were determined using an Aurora M90 inductively coupled plasma mass spectrometer (ICP-MS, Bruker, Germany). Samples were transferred into solution by autoclave decomposition before the ICP-MS measurements. Various acids or their mixtures in the form of concentrated HNO_3 or other acids (such as HCl, $HClO_4$, and H_2SO_4) and a solution of H_3BO_3 diluted with deionized water were used to obtain an effective precipitate during digestion. Samples of 0.1 g were used for the analysis. Standard samples of the Institute of Geochemistry of the Siberian Branch of the Russian Academy of Sciences (Irkutsk, Russia) were treated similarly and used to check the correctness of the sample analysis.

The ochre samples were further studied by X-ray diffraction (XRD) to determine the presence of crystalline phases in them and their diagnosis. A total of 10 ochre samples of different types were studied using a D2 Phaser powder XRD (Bruker, Germany) equipped with an X-ray tube with a copper anode (emitting CuKα, $\lambda = 1.54060$ Å), a generator with 30 kV, and 10 mA current, a LYNX EYE line detector, and a Ni filter. Imaging conditions: the divergent slit was 0.6 mm, Soller slits were primary 2.5°, secondary 2.5°; angular range 2θ was from 5 to 70°; pulse set rate at each point was 1.0 s; step was 0.03. Curve processing (smoothing, searching for peaks), qualitative analysis, and semi-quantitative analysis were performed using Diffrac.Eva program. The PDF-2 (2010 release) powder diffractometry database was used to search for mineral phases.

Finally, representative varieties of ochre were selected from the 0.25–0.1 mm class for SEM studies. To preserve the individual features of the ochre microtexture, preparations were made with minimal mechanical impact, which somewhat affected the clarity of the photographs. The preparations were sprayed with carbon.

The main purpose of the SEM studies was to establish the morphological features, the aggregate structure of the ochre particles, and to determine the chemical composition of individual fragments of aggregates by microprobe analysis. Images with relatively low magnification were used to study the morphological features and surfaces of the ochre particles were obtained using a JSM 6390LV (Jeol, Tokyo, Japan). The operating mode of the microscope was 10 mA, operating voltage was 20 kV, and the working distance was 12 mm. Local microanalysis of the ochre aggregates was performed using the INCA ENERGY 350 (Oxford Instruments, Abingdon, UK). Samples of oxides and metals manufactured by Jeol were used as standards.

SEM observations revealed heterogeneity in the structure of ochre particles, which include μm-sized grains, the substance cementing them, as well as microaggregates composed of nanosized particles. Local microanalysis was used exclusively to determine the chemical composition of microaggregates composed of nanoparticles. A total of 30 microprobe analyses were performed.

A detailed study of the morphology and interrelation of micro- and nanoparticles within the above microaggregates was performed using a high-resolution cold-emission JSM 7500F SEM (Jeol, Tokyo, Japan). The modes of operations: a current strength of 20 mA, working voltage of 10 kV, and a working distance of 8 mm.

Results and Discussion

Typification of Ochre Particles

The study of ochre particles under a binocular microscope shows that they differ in many ways (colour, shape of excretions, character of surface, hardness, and mechanical strength; Fig. 4). Considering the morphological features and visual differences in the texture, the following types of ochre particles can be distinguished:

1) *Aggregates,* consisting of clay particles, quartz and feldspar grains, small fragments of coal, etc., and ochre cement, are mainly characteristic of the larger size classes. Their colour varies from dark brown to red, the

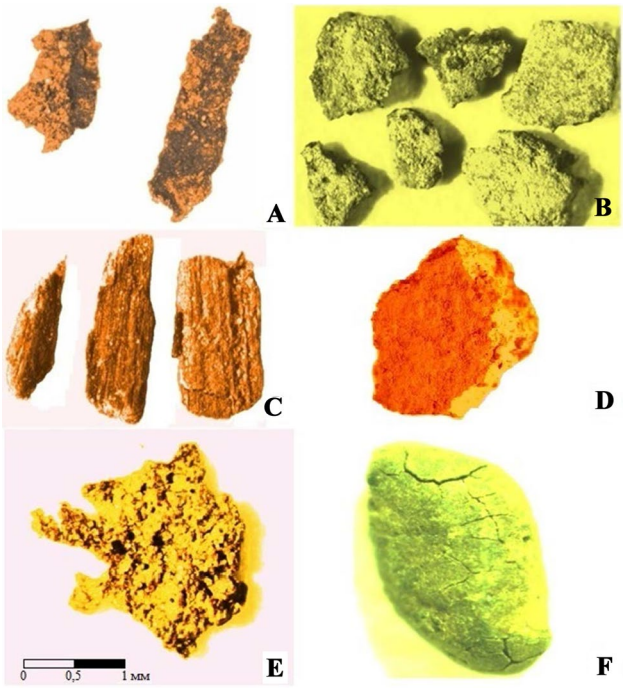

Fig. 4 Main types of ochre particles: **A** plate-like coal particles with ochres on the surface; **B** aggregates cemented with ochre formations; **C** pseudomorphosis after wood; **D** film on the surface of the quartz grain; **E** microaggregates; **F** kidney-like secretions

shape of the grains is rounded, lumpy, etc. These formations, heterogeneous in composition, are characterized by weak roundness, increased hardness, and mechanical strength.

2) *Pseudomorphs after wood* are characterized by a fibrous structure, thinly ribbed surface, yellowish-red or reddish-brown colouration, flattened and elongated appearance of grains, and splintery fractures at the ends. They are predominantly in the coarse- and medium-sized sediment classes.
3) *Microaggregates of iron hydroxides* are bright yellow or reddish-yellow colour with a fine-grained microtexture. They are extremely fragile and concentrate in small-sized classes (< 0.25 mm).
4) *Crusts* of red, yellow, or brown colour exist on the surface of lamellar particles of coal or metal shavings, formed by precipitation of ferrous matter from river sediments.
5) *Kidney-like formations* are characterized by an oval shape and brown or reddish colouring with cracks on the surface. Their formation is most likely due to precipitation from colloidal solutions around the centres of crystallization, which can be various mineral grains.
6) *Film-like precipitates* on the surface of clastic grains (quartz, feldspar, hematite, chromite, pyroxenes, rock fragments, etc.).

The first three types are usually the most common, but others are also present in appreciable quantities at some sampling sites. The morphological type of ochre particles is an indicator of the conditions of their formation; in particular, it is related to the facies setting of sedimentation. The diversity of morphological types indicates a variety of natural-technogenic facies conditions of sedimentation in zones of anthropogenic impact on natural sediments.

Occurrence of Ochre in Sediments

Considerably more ochre particles were noted in river sediments directly near where the coal mine water discharges, and in the coastal zone here there are coal mine dumps. Here, the content of ochre particles in the bottom sediments peak at ≈ 80%, while in the downstream Kosva River sediment, there is no more than 9%, and in some cases even < 1% (Table 2).

An important result is the sharp variability in ochre particle content in the Gubakha area sediments, which at some sampling points decreases to ≤ 3%. This may be due to an important difference in the geochemical conditions in which the ochre precipitates. The facies conditions of sedimentation, tributaries, anthropogenic activity, etc. also have an influence.

For the territory outside the influence of coal mining, the bottom sediments of the Kosva River contain iron aggregates, which morphologically and structurally resemble ochre particles (≈ 1%). Apparently, iron hydroxides are present here as characteristic mineral components of river sediments in the Ural region.

Size of Ochre Particles

In the Gubakha area, the highest concentration of ochre particles was found in the coarse size classes (> 0.5 mm). Particles of this size account for most of the sharply increased content of ochre in sediments. Near the mine discharges, there are sediments almost entirely composed of debris, grains, and fine flakes of ochre.

In the downstream area of the Kosva River, along with a tendency for a general decrease in the total content of ochre particles in sediments, the bulk of these formations are in the small-sized classes (< 0.25 mm). This is due to the low migration capacity of large ochre particles. In addition, it should be concluded that ochres particles in the downstream sediments came from the coal mining areas, rather than forming at the sampling site (Table 2).

Table 2 Ochre particles content in the size classes of sediments of the Kosva River, vol. %

Sample	Value range, mm						Total, %
	> 1.0	1.0–0.5	0.5–0.25	0.25–0.1	0.1–0.05	< 0.05	
Above the impact of coal mine development							
1	1	1	1	3	7	5	1, 1
The area around the town of Gubakha							
2	100	90	85	70	65	60	80.0
3	25	10	7	5	10	3	6.3
4	2	2	3	5	7	5	2.7
5	1	10	15	25	30	10	7.3
6	85	70	60	35	30	25	59.7
7	65	75	50	40	35	25	41.6
8	–	100	90	50	35	20	36.1
9	30	35	40	40	35	25	30.9
10	30	25	15	20	25	15	22.5
11	–	3	5	35	58	53	13.5
12	2	70	64	63	49	37	7.8
Downstream of the Kosva River							
13	1	2	3	3	2	2	0.6
14	3	5	51	65	69	66	8.7
15	1	2	3	6	30	25	3.7

Microtexture of Ochre Particles

The SEM study of aggregate ochre particles ranging in size from 0.25 to 0.1 mm in the magnification range from a few to 20 thousand times revealed their great diversity. The was a marked difference in the microtexture of the ochre particles, which may indicate some peculiarities of their genesis. The most widespread are the highly porous aggregates; at a magnification of 2000–5500, dense clusters of 20–30 μm aggregates, composed of elongated or rounded particles several μm in size, are clearly seen. Between them, there is a noticeable volume of void space (supplemental Fig. S-1).

Images with a magnification of 10–20 thousand times reveal clusters composed mainly of discrete particles less than 1 μm in size composed of individual microaggregates (supplemental Fig. S-2). At the same time, very dense packing of these particles allows us to assume that between them there is a cementing substance. At this magnification, a wide distribution of microcavities of different shapes and lengths in ochre particles becomes noticeable.

For the pseudomorphs after wood, the SEM images clearly show morphological signs of their fibrous texture inherited from primary wood particles. The thickness of the individual fibres does not exceed 1 μm (supplemental Fig. S-3). The fibres are observed in cross-sectional view as well (supplemental Fig. S-4). In contrast to the highly porous aggregates, these pseudomorphs are much denser and more homogeneous in structure. However, they are characterized by the presence of extended slit-like voids along the fibres. Some of them may be filled with secondary minerals.

Nanotexture of Ochre Particles

For the first time, the nanoscale value of the constituent particles of microaggregates in highly porous ochre particles can be detected. At magnifications of the order of 50–75 thousand, the microstructure of most of the ochre particles appears as a set of microaggregates from 1 to 0.2 μm in size, which, in turn, are clusters of nanoparticles or nanoaggregates < 100 nm in size (supplemental Fig. S-5).

Two types of microaggregate nanotextures are clearly distinguished: (1) porous structure with isometric nanoparticles and voids between their clusters; and (2) dense structure with worm-shaped aggregates of nanoparticles and cementing substance between them. Nanotextures of the first type are characterized by local clusters of nanoparticles forming various microaggregates. In the second type, the worm-like excretions form microaggregates of complex shape with the presence of important (in the nanoscale range) distances between them, filled with a dense mass of the cementing substance.

At magnifications of 100,000 times, the sizes of nanoparticles in porous microaggregates differ appreciably. Some of them are composed of nanoparticles of ≈ 20–30 nm in size, while others are larger (50–75 nm; supplemental Fig. S-6). The difference is also evident in the structure and volume of the void space between the clusters of nanoparticles.

Under the same magnification, the details of their complex nanotexture can be seen in ochres with worm-like aggregates of nanoparticles and cement matter. The worm-like aggregates are often ≥ 500 nm in length and ≈ 75–150 nm across. They are usually composed of nanoparticles ≤ 50 nm, cemented by a binding agent into very dense branching flagella (supplemental Fig. S-7). The nanogranular texture of the basal cementitious mass with a particle size < 10 nm can also be traced (supplemental Fig. S-8).

Chemical Composition of Ochre Particles

Trace Elements

According to the ICP-MS results, Zn, Ni, Cu, Pb, Co, and As were the most abundant trace elements in the studied ochre particles. Their concentration was usually less than 0.01% (Table 3). Cd, Sb, and Hg are present in markedly lower amounts. The ochre particles in the Gubakha area and the downstream Kosva River differ markedly in their trace elements associations. In particular, the ochre particles in the Gubakha area contain importantly more Co, Ni, Pb, and Sb, i.e., typical trace elements in pyrite. The ochre particles in the downstream of the Kosva River had a relatively elevated Cd content, which could be due to erosion in the middle and lower reaches of the river.

Chemical Composition of Nanoparticle Microaggregates

In addition, microprobe analysis was used (24 analyses, 12 samples) to determine the specificity of the material composition of nanoparticle microaggregates in the ochre particles. They are of great interest as the earliest components of ochre formation, which were later cemented by a binder. The chemical composition was determined at two points of individual microaggregates, in which their nanoscale structure was clearly traced (Tables 4 and 5).

The most important difference between the chemical composition of the microaggregates and the total chemical composition of the ochre particles is the noticeable predominance of iron oxides (Table 4). Other components present in appreciable amounts include silica, alumina, phosphorus, and sulphur oxides. In rare microaggregates, the CaO content is slightly increased.

In the microaggregates of ochre particles in the Gubakha area, a particularly high content of iron oxides (more than 60%, sometimes up to 86% and more) was observed; an increased sulphur content was also characteristic, and in some microaggregates, silica and alumina. The ochre microaggregates of the lower Kosva River contained considerably less iron oxide and more silica and had higher phosphorus and calcium concentrations. Comparison of these data suggests that jarosite is present among the nanoparticles in the ochre microaggregates of the Gubakha area and vivianite is present in those of the downstream Kosva River.

Another important difference between the chemical composition of the microaggregates and bulk ochre particles was the sharply increased (by two or three orders of magnitude) content of such trace elements as copper and zinc. The constant presence of copper and zinc in ochres in approximately equal concentrations (see Tables 4 and 5) and close correlation between them (Fig. 5) testify to their common origin and a single primary source. Evidently, this primary source was pyrite in the coal-bearing rocks. During pyrite decomposition, copper and zinc ions are released from pyrite in addition to formed iron hydroxides. This has also been proven by experimental studies with prolonged (for 2 years) leaching of pyrite (Nyström et al. 2021). Iron hydroxides, copper, and zinc pass into colloidal solutions as a solid phase (micelles).

The coagulation of colloidal solutions results in the co-precipitation of iron hydroxides and copper and zinc compounds. The histograms of copper and zinc concentrations in ochre (50 microprobe analyses) were unimodal, which

Table 3 Concentrations of trace elements in ochre particles, ppm

Elements	The area around the town of Gubakha				Downstream of the Kosva River		
	Sample site						
	9	10	11	12	13	14	15
Cu	28.5 ± 6.8	34.1 ± 8.2	23.6 ± 5.7	33.3 ± 8.0	30.2 ± 7.2	31.8 ± 7.6	24.1 ± 5.8
Zn	76.6 ± 18.4	88.4 ± 21.2	32.4 ± 7.8	47.9 ± 11.5	91.6 ± 22.0	105.9 ± 25.4	60.4 ± 14.5
Co	15.3 ± 4.6	14.0 ± 4.2	5.65 ± 1.7	13.0 ± 3.9	20.0 ± 4.8	35.2 ± 8.4	18.1 ± 5.4
Ni	34.8 ± 8.4	38.5 ± 9.2	19.0 ± 5.7	29.5 ± 7.1	45.3 ± 10.9	50.9 ± 12.2	41.3 ± 9.9
Pb	18.3 ± 5.5	21.0 ± 5.0	9.1 ± 2.7	23.4 ± 5.6	12.4 ± 3.7	11.6 ± 3.5	9.1 ± 2.7
As	13.3 ± 6.7	12.8 ± 6.4	9.9 ± 5.0	9.0 ± 4.5	9.4 ± 4.7	10.1 ± 5.1	8.1 ± 4.1
Cd	1.12 ± 0.46	1.04 ± 0.43	0.52 ± 0.21	0.93 ± 0.38	1.57 ± 0.64	1.90 ± 0.78	1.64 ± 0.67
Sb	0.60 ± 0.36	0.66 ± 0.40	0.74 ± 0.44	0.90 ± 0.54	0.56 ± 0.34	0.61 ± 0.37	0.43 ± 0.26
Hg	0.18 ± 0.11	0.25 ± 0.15	0.03 ± 0.02	0.04 ± 0.02	0.10 ± 0.06	0.18 ± 0.11	0.05 ± 0.03

Table 4 Chemical composition of microaggregates in ochre particles (the area around the town of Gubakha), wt%

Component	Sample and microaggregate number									
	2		**3**		**5**		**6**		**7**	
	1	*2*	*3*	*4*	*5*	*6*	*7*	*8*	*9*	*10*
Fe_2O_3[a]	74.12	83.03	65.7	76.58	84.47	84.14	76.17	73.82	76.32	76.96
SO_3	10.86	9.71	5.07	6.78	1.17	2.2	20.82	22.57	4.72	2.74
V_2O_5	0.05	–	–	–	0.05	–	0.09	0.07	0.05	–
P_2O_5	–	–	0.18	0.27	0.06	–	–	0.14	0.1	–
SiO_2	0.71	0.48	16.11	6.21	0.52	1.97	0.63	0.77	6.01	8.15
TiO_2	–	–	–	–	0.04	0.08	–	–	–	0.16
Al_2O_3	10.62	3.8	7.79	5.33	7.47	5.87	0.96	0.92	8.17	6.7
CaO	0.09	0.07	0.96	0.89	1.22	1.34	0.05	0.13	1.08	0.96
MgO	–	–	0.82	0.7	0.15	–	–	0.25	0.57	0.63
MnO	–	–	0.08	0.06	0.1	0.11	–	–	0.08	0.09
K_2O	–	–	0.31	–	0.06	0.1	0.31	0.06	0.08	0.29
Na_2O	0.21	–	–	–	0.09	–	–	–	–	–
Cu	1.31	1.09	1.08	1.15	1.86	1.72	0.25	0.42	0.98	1.32
Zn	1.13	0.95	1.03	1.02	1.52	1.32	0.19	0.33	0.94	1.07
Co	0.24	0.23	0.27	0.29	0.2	0.19	0.23	0.17	0.26	0.15
Ni	–	0.06	–	0.07	0.07	–	0.06	0.04	–	0.07
Sb	–	–	–	–	–	0.09	–	–	–	–
As	–	–	–	–	–	–	–		–	–
Cl	–	–	–	–	0.04	0.04	0.05	0.08	0.08	0.05
	9		**10**		**11**		**12**			
	13	*14*	*15*	*16*	*17*	*18*	*19*	*20*		
Fe_2O_3[a]	70.54	86.4	78.46	65.27	82.61	69.61	64.89	75.39		
SO_3	4.62	6.76	8.43	9.35	7.56	12.74	2.38	0.91		
V_2O_5	–	–	0.08	–	–	0.05	–	–		
P_2O_5	–	–	0.13	0.17	–	–	0.34	0.21		
SiO_2	16.09	2.57	7.13	19.64	3.67	7.99	12.77	9.59		
TiO_2	0.14	0.07	0.1	0.09	0.22	0.09	0.06	0.04		
Al_2O_3	3.89	1.45	3.44	4	3.02	5.62	10.8	6.29		
CaO	–	0.08	0.22	–	–	0.07	3.07	3.85		
MgO	0.41	–	0.36	0.51	–	0.44	1.08	0.76		
MnO	–	–	–	–	–	–	0.05	0.1		
K_2O	2.03	0.32	0.7	0.29	1.53	0.59	0.32	0.24		
Na_2O	0.15	0.21	0.21	–	–	–	–	0.15		
Cu	0.82	0.76	0.14	0.16	0.35	1.08	1.58	1.04		
Zn	0.73	0.81	0.19	0.13	0.38	0.85	1.56	0.93		
Co	0.15	0.11	0.17	0.16	0.26	0.18	–	–		
Ni	–	–	0.04	0.06	0.08	–	–	0.05		
Sb	–	–	–	–	–	–	0.2	–		
As	–	–	–		–	0.07	–	–		
Cl	0.03	0.04	0.06	0.03	0.04	0.05	0.08	–		

[a]$Fe_2O_3 + FeO$

Table 5 Chemical composition of microaggregates in ochre particles (downstream of the Kosva River), wt. %

Component	Sample and microaggregate number					
	13		14		15	
	21	*22*	*23*	*24*	*25*	*26*
Fe_2O_3[a]	43.13	37.63	38.56	22.52	63.42	65.98
SO_3	0.57	1.47	0.76	0.40	0.34	0.34
P_2O_5	1.09	1.38	0.91	0.31	5.63	17.30
V_2O_5	–	–	0.06	0.04	0.06	0.05
SiO_2	26.74	40.07	32.90	48.39	17.47	6.32
TiO_2	0.45	0.28	0.57	0.36	0.05	–
Al_2O_3	14.88	0.28	15.48	17.65	6.26	1.13
CaO	3.25	3.47	4.54	2.60	2.16	4.91
MgO	1.08	1.69	2.03	2.41	1.15	–
MnO	0.19	0.07	0.11	0.12	0.07	0.13
K_2O	0.96	0.75	1.03	1.85	0.17	0.06
Na_2O	0.63	0.43	0.98	1.67	0.15	–
Cu	0.99	1.06	0.64	0.58	0.98	0.87
Zn	1.32	1.32	0.84	0.63	1.29	1.05
As	–	0.10	–	–	–	0.09
Sb	0.23	0.20	0.18	0.10	0.10	0.10
Ni	0.07	0.09	0	0.04	–	–
Co	–	–	–	–	–	0.19
Cl	0.05	0.13	–	0.05	0.13	0.10
Hg	–	–	0.13	–	–	–

[a]$Fe_2O_3 + FeO$

is another confirmation that these metals have a common primary source, the coal-bearing formation rocks (Fig. 6).

However, it should be noted that there is no direct correlation between the concentrations of iron oxides and the above metals. For example, at low FeO* concentrations, there may be very high concentrations of copper and zinc and vice versa (see Tables 4 and 5). This could be due to the presence of other sources of iron in the geological environment in addition to pyrite, in which copper and zinc are absent. These may be ferruginous chlorites, siderite deposits, and ferruginous sandstones.

The concentrations of copper and zinc vary markedly even within a single microaggregate in ochre particles (Table 6). This is due to the presence of clay minerals, salts, carbonates, and sulphates in addition to iron hydroxides. Elevated concentrations of copper (> 2%) and zinc (≈ 2%) were observed in the iron hydroxide microaggregates, which were characterized by low silicon content (Fig. 7).

Among other trace elements, cobalt was typical for ochres in the Gubakha area and antimony in ochres from the lower course of the Kosva River. Nickel was recorded in many analyses, and arsenic and mercury in some. The most probable source of these metals was once again the pyrite. They are presumably sorbed by ferrous matter, primarily by nanoparticles within the microaggregates.

According to Nowack and Sigg (1996), the sorption of cationic metals on the surface of iron hydroxides is explained by surface complexation by covalent bonds with the surface OH-groups. The sorption of metals (Pb, Cu, Cd, Ni, etc.) on various surfaces increases with increasing solution pH.

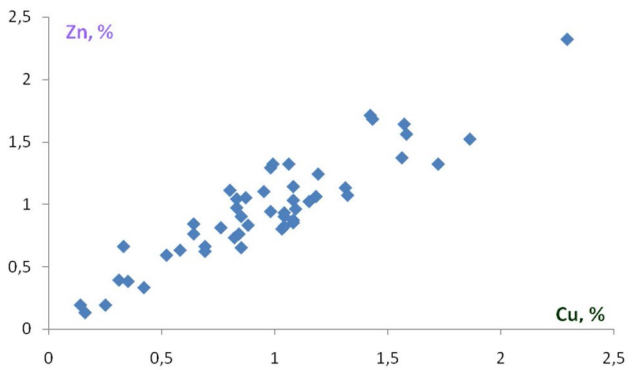

Fig. 5 Relation between copper and zinc contents in ochre microaggregates

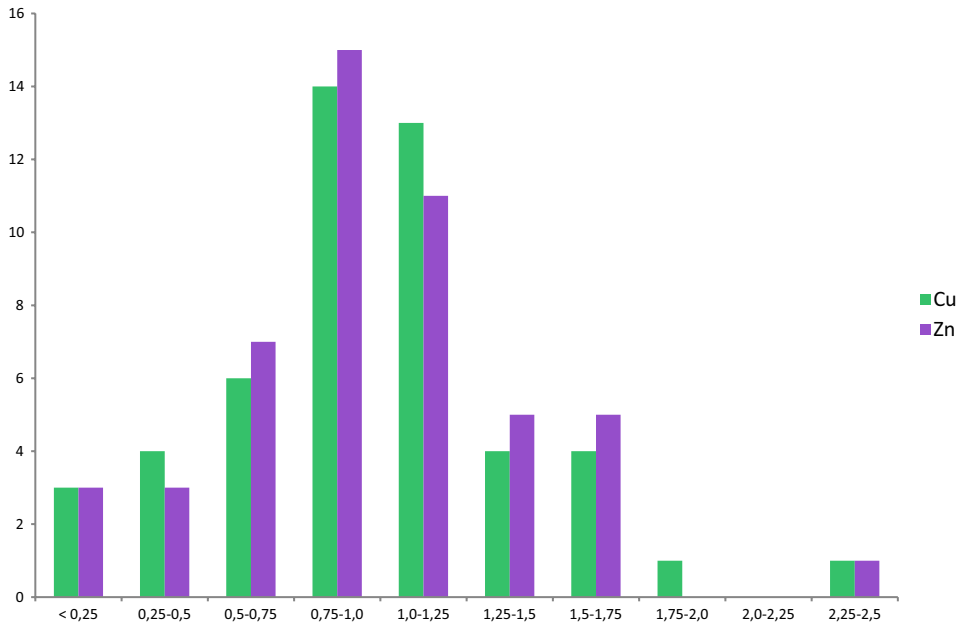

Fig. 6 Histogram of copper and zinc content distribution (%) in ochre microaggregates

Table 6 Concentration of elements in individual points of ochre microaggregate (sample 6), wt. %

Elements	Point number									
	1	2	3	4	5	6	7	8	9	10
Cu	1.25	1.52	1.54	1.58	1.60	1.94	2.01	2.26	2.34	2.56
Zn	1.08	1.24	1.20	1.27	1.30	1.95	1.69	1.91	1.85	2.04
Fe	27.87	41.33	58.27	28.33	58.24	23.03	63.01	55.48	54.87	54.70
Si	15.55	10.40	2.98	18.92	3.80	5.07	1.35	2.68	2.08	2.72
Al	8.44	5.95	3.16	5.50	2.79	3.16	1.78	4.34	5.30	4.57
S	1.13	1.68	2.15	0.99	1.58	1.13	1.55	2.01	2.38	2.06

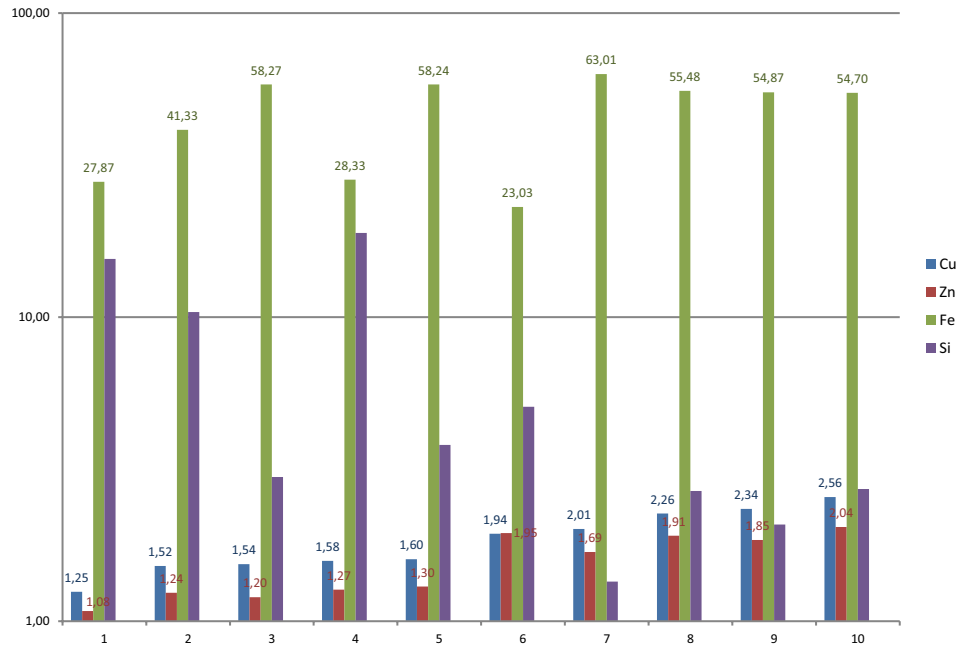

Fig. 7 Ratio of concentrations of Zn, Cu, Fe, and Si (%) in individual points of ochre microaggregate (sample 6)

Table 7 Semi-quantitative mineralogical composition of the crystalline part of the typical ochre samples estimated by XRD, wt. %

Minerals	Sampling sites									
	The area around the town of Gubakha							Downstream of the Kosva River		
	2	5	7	9	10	11	12	13	14	15
Quartz	88	48	53	40	41	44	66	43	54	58
Plagioclases	4	8	10	10	12	15	4	22	20	22
Potassium feldspar	3	10	13	20	18	14	7	11	9	12
Mica	–	15	13	8	12	22	18	23	13	2
Chlorite	–	9	7	8	9	–	–	–	3	4
Hematite	–	3	1	3	3	–	3	–	–	–
Goethite	5	2	2	8	5	2	1	1	1	2
Calcite	–	3	1	3	–	3	–	–	–	–
Jarosite	–	2	–	–	–	–	2	–	–	–
Amount	100	100	100	100	100	100	100	100	100	100

Mineral Composition of the Ochre Particles

The mineral composition of the crystalline part of the ochre matter (Table 7), which was established using XRD, testifies to the presence in the ochre formations of a complex mineral association of different components and genesis: clastic particles of terrigenous sedimentary rocks (quartz, feldspars, plagioclases), clay particles of fluvial suspensions (mica, chlorite), components of binding and cementing matter (goethite, calcite), and characteristic minerals (jarosite).

The quantitative ratio of mineral components in the ochre composition varied markedly. Quartz was the predominant mineral. Feldspars and clay minerals and plagioclases accounted for a notable portion of the crystalline matter in almost all the ochre particles.

The composition of ochre in the Gubakha area and in the downstream part of the Kosva River was markedly different. Higher goethite and hematite contents (up to 8%) were noted in the ochre of the Gubakha area. Here, hematite and calcite and jarosite were also diagnosed in ochre by XRD.

According to the general appearance of diffractograms, all the studied ochre samples can be divided into two groups: (1) with a relative variety of crystalline substances; (2) with a limited variety of crystalline substances (supplemental Figs. S-9, S-10). At the same time, due to the dynamics of the ochre sediments, in most samples a certain portion of their substance is in the latently crystalline state.

High-resolution SEM data demonstrate the wide presence of nanoparticles in the ochre composition, the corresponding part of which was not diagnosed by XRD. The mineral composition of the crystalline part of the nanoscale matter can be indirectly judged by the microprobe analysis data (see Tables 4 and 5). In microaggregates with greater sulphur and phosphorus content, we can assume the presence of jarosite and vivianite occurred a cryptocrystalline form.

Conclusions

Ochres are common by-products of mining in the study area. The abundance of pyrite and organic sulphur in the coal-bearing deposits is the reason for the abundance of ochre particles in the bottom sediments of the rivers of the Kizel coal basin. Ochre sediments are secondary mineral formations that form directly as a result of sedimentation from acid sulphate waters in watercourses, mine water discharge channels, and waste rock dumps.

Ochre particles are complex polymineral and polygenetic aggregates. They consist of four major components: clastic particles, clay matter, cementing material, and microaggregates of nanoparticles. Quartz, feldspars, and plagioclases were the most common clastic particles. Their primary sources were local rocks (sandstones, siltstones, and basic igneous complexes). They are small (tens of μm) and flattened in shape, which makes them highly migratory. Their settling under floodplain water flow conditions is caused by extremely low settling velocity. The clayey rocks of the geological environment (argillites and clay shales), which are typical components of suspended sediments, are the primary sources of clay particles (micas and chlorites).

Ferruginous, sulphate, carbonate, and phosphate formations serve as the cementing substance in ochre aggregates. Their transfer occurred primarily in the colloidal state, with deposition occurring during colloidal aging or at a specific geochemical barrier.

The main characteristic of the ochre structure is its fine dispersion; a portion of the substance is in a nanoscale state. Nanoparticles are known to have a high sorption capacity, which is confirmed by elevated concentrations of toxic elements in nanoparticle microaggregates (in wt.%): Cu ($\leq$2.56), Zn ($\leq$2.04), Co ($\leq$0.29), Sb ($\leq$0.23), Hg ($\leq$0.13), and As ($\leq$0.10).

All indications, including the bright red or yellow colour of the river water, which does not clear for tens of km, point to the high migratory ability of the ochre substance. Floodplain sediments on the shallows, as well as river channel sediments, stand out with their bright red colour. An important portion of the nanosized substance becomes a component of colloidal solutions, while larger particles are transferred as suspended particles. For the Kosva River, the observed interval of ochre migration was more than 100 km. Space images clearly visualize the zone of influence of the river flow on the Kama reservoir, which is at least 30 km further. This poses for us the task to further investigate sedimentation processes in the water area of the Kama reservoir.

Evidence also suggests that the ochres in these areas were of different origins. The mineral composition of the ochre particles changed noticeably with distance from the mining area.

The findings provide once more a foundation for researchers to focus their attention on nanosized phases in the composition of river sediments as toxic element sorbents. As active migrants in watercourses, ochre formations transport toxic elements and contribute to their widespread distribution in water bodies and floodplains across large areas. The possibility of their accumulation in final reservoirs of river runoff (in our case, the Kama Reservoir) is especially dangerous. As the main concentrator of toxic elements, ochre sediments require special attention in monitoring studies.

Supplementary Information The online version contains supplementary material available at https://doi.org/10.1007/s10230-022-00905-3.

Acknowledgements This research was supported by the Perm Research and Education Centre for Rational Use of Subsoil, 2022.

Data Availability The authors (E. Menshikova, B. Osovetsky, S. Blinov, P. Belkin, E. Tomilina, I. Badyanova) confirm the availability of the data used in preparing this article.

References

Acharya B, Kharel G (2020) Acid mine drainage from coal mining in the United States–an overview. J Hydrol 588:125061. https://doi.org/10.1016/j.jhydrol.2020.125061

Benton MJ (2012) No gap in the middle Permian record of terrestrial vertebrates. Geology 40:339–342. https://doi.org/10.1130/G32669.1

Berezina OA, Shikhov AN, Abdullin RK (2018) Application of multiyear series of space imagery data to assess the environmental situation in coal-mining areas (on the example of the liquidated Kizel coal basin). Curr Probl Earth Remote Sens Space 15(2):144–158. https://doi.org/10.21046/2070-7401-2018-15-2-144-158(inRussian)

Butt C, Cluzel D (2013) Nickel laterite ore deposits: weathered serpentinites. Elements 9(2):123–128. https://doi.org/10.2113/gselements.9.2.123

Campaner VP, Luiz-Silva W, Machado W (2014) Geochemistry of acid mine drainage from a coal mining area and processes controlling metal attenuation in stream waters, southern Brazil. An Acad Bras Cienc 86:539–554. https://doi.org/10.1590/0001-37652014113712

Carbone C, Dinelli E, Marescotti P, Gasparotto G, Lucchetti G (2013) The role of AMD secondary minerals in controlling environmental pollution: indications from bulk leaching tests. J Geochem Explor 132:188–200. https://doi.org/10.1016/j.gexplo.2013.07.001

Consani S, Carbone C, Dinelli E, Balić-Žunić T, Cutroneo L, Capello M, Salviulo G, Lucchetti G (2017) Metal transport and remobilisation in a basin affected by acid mine drainage: the role of ochreous amorphous precipitates. Environ Sci Pollut Res 24:15735–15747. https://doi.org/10.1007/s11356-017-9209-9

Copaja SV, Mauro L, Vega-Retter C, Véliz D (2020) Adsorption-desorption of trace elements in sediments of the Maipo river basin. J Chil Chem Soc 65(2):4778–4783. https://doi.org/10.4067/S0717-97072020000204778

Cravotta CA (2008) Dissolved metals and associated constituents in abandoned coal-mine discharges, Pennsylvania, USA. Part 1: constituent quantity and sand correlations. J Appl Geochem 23(2):166–202. https://doi.org/10.1016/j.apgeochem.2007.10.011

Dauvalter VA (2012) Geoecology of lake sediments. Murmansk STU Publisher, Murmansk (**in Russian**)

Dvinskikh SA, Vostroknutova YO, Kitaev AB (2015) The role of technogenic iron in the formation of its content in the water of the Kamskoye and Votkinskoye reservoirs. Geographic Bull 4(35):18–25 (**in Russian**)

Equeenuddin SM, Tripathy S, Sahoo PK, Panigrahi MK (2010) Geochemistry of ochreous precipitates from coal mine drainage in India. Environ Earth Sci 9:113–116. https://doi.org/10.1007/s12665-009-0386-9

Erguler ZA, Erguler GK (2015) The effect of particle size on acid mine drainage generation: kinetic column tests. Miner Eng 76(15):154–167. https://doi.org/10.1016/j.mineng.2014.10.002

Espana JS, Pamo EL, Santofimia E, Aduvire O, Reyes J, Barettino D (2005) Acid mine drainage in the Iberian Pyrite Belt (Odiel river watershed, Huelva, SW Spain): Geochemistry, mineralogy and environmental implications. Appl Geochem 20(7):1320–1356. https://doi.org/10.1016/j.apgeochem.2005.01.011

Espana JS (2007) The behavior of iron and aluminum in acid mine drainage: speciation, mineralogy, and environmental significance. In: Letcher TM (ed) Thermodynamics solubility and environmental issues. Elsevier, pp 137–150. https://doi.org/10.1016/B978-044452707-3/50009-4

Grazhdankin DV, Maslov AV (2015) The room for the Vendian in the international chronostratigraphic chart. Russ Geol Geophys 56:549–559. https://doi.org/10.1016/j.rgg.2015.03.007

Grazhdankin DV, Maslov AV, Krupenin MT (2009) Structure and depositional history of the Vendian Sylvitsa group in the western flank of the central urals. Stratigr Geo Correl 17:20–40. https://doi.org/10.1134/S0869593809050025

Harraz HZ (2013) Sedimentary manganese and iron ore deposits. Course of lectures, Topic 3. Available online on Researchgate: https://doi.org/10.13140/RG.2.1.1822.2967

Herr C, Gray NF (1996) Seasonal variation of metal contamination of riverine sediments below a copper and sulphur mine in southeast Ireland. Water Sci Technol 33(6):255–261. https://doi.org/10.1016/0273-1223(96)00294-6

Imaikin A (2014) Mine waters of Kosva field of Kizel coal basin during and after its operation, forecast of hydrochemical regime of mine waters that are discharged on the surface. In: Proceedings of the International Multidisciplinary Scientific GeoConference Surveying Geology and Mining Ecology Management (SGEM2014), Albena, Bulgaria, pp 605—612

INAP (The International Network for Acid Prevention) Global Acid Rock Drainage (GARD) Guide. Available online: http: //www.

gardguide.com/images/5/5f/TheGlobalAcidRockDrainageGuide.pdf (Accessed 6 Aug 2021).
Jamieson HE, Walker SR, Parsons MB (2015) Mineralogical characterization of mine waste. Appl Geochem 57:85–105. https://doi.org/10.1016/j.apgeochem.2014.12.014
Jönsson J, Jönsson J, Lövgren L (2006) Precipitation of secondary Fe(III) minerals from acid mine drainage. Appl Geochem 21(3):437–445. https://doi.org/10.1016/j.apgeochem.2005.12.008
Kefeni KK, Msagati TAM, Mamba BB (2017) Acid mine drainage: prevention, treatment options, and resource recovery: a review. J Clean Prod 151:475–493. https://doi.org/10.1016/j.jclepro.2017.03.082
König U (2021) Nickel Laterites—Mineralogical monitoring for grade definition and process optimization. Minerals 11(11):1178. https://doi.org/10.3390/min11111178
Kotlyar GV (2015) Permian sections of southern primorye: a link in correlation of stage units in the standard and general stratigraphic scales. Russ J Pacific Geol 9:254–273. https://doi.org/10.1134/S1819714015040041
Kumpulainen S, Carlson L, Raisanen M-L (2007) Seasonal variations of ochreous precipitates in mine effluents in Finland. Appl Geochem 22(4):760–777. https://doi.org/10.1016/j.apgeochem.2006.12.016
Kupka D, Pállová Z, Horňáková A, Achimovičová M, Kavečanský V (2012) Effluent water quality and the ochre deposit characteristics of the abandoned Smolník mine. East Slovakia Acta Montan Slovaca 17(1):56–64
Lottermoser BG (2007) Mine wastes Characterization, Treatment, Environmental Impacts, 2nd edn. Springer, New York
Lozovsky VR, Minikh MG, Grunt TA, Kukhtinov DA, Ponomarenko AG, Sukacheva ID (2009) The Ufimian stage of the East European scale: status, validity, and correlation potential. Stratigr Geo Correl 17:602–614. https://doi.org/10.1134/S0869593809060033
Lucas SG, Shen S (2016) The Permian chronostratigraphic scale: history, status and prospectus. Special Publ 450:21–50. https://doi.org/10.1016/10.1144/SP450.3
Lyubimova T, Parshakova Y, Lepikhin A, Tiunov A (2016) The risk of river pollution due to washout from contaminated floodplain water bodies during periods of high magnitude floods. J Hydrol 534:579–589. https://doi.org/10.1016/j.jhydrol.2016.01.030
Marescotti P, Carbone C, Comodi P, Frondini F, Lucchetti G (2012) Mineralogical and chemical evolution of ochreous precipitates from the Libiola Fe-Cu-sulfide mine (eastern Liguria, Italy). Appl Geochem 27(3):577–589. https://doi.org/10.1016/j.apgeochem.2011.12.024
Maximovich N, Khayrulina E (2014) Artificial geochemical barriers for environmental improvement in a coal basin region. Environ Earth Sci 72:1915–1924. https://doi.org/10.1007/s12665-014-3099-7
Menshikova E, Osovetsky B, Blinov S, Belkin P (2020) Mineral formation under the influence of mine waters (the Kizel Coal Basin, Russia). Minerals 10:364. https://doi.org/10.3390/min10040364
Nordstrom DK (2011) Hydrogeochemical processes governing the origin, transport and fate of major and trace elements from mine wastes and mineralized rock to surface waters. Appl Geochem 26(11):1777–1791. https://doi.org/10.1016/j.apgeochem.2011.06.002
Nowack B, Sigg L (1996) Adsorption of EDTA and metal-EDTA complexes onto goethite. J Colloid Interface Sci 177:106–121. https://doi.org/10.1006/jcis.1996.0011
Nyström E, Thomas H, Wanhainen H, Alakangas L (2021) Occurrence and release of trace elements in pyrite-rich waste rock. Minerals 11(5):495. https://doi.org/10.3390/min11050495
Plyusnin AV, Sulima AI, Timofeev VD, Koval DV, Dementyeva KV (2021) Lithological-facial structure of the Ufimian sediments in the central part of the Perm Krai. Bull Tomsk Polytech u Geo Assets Eng 332:29–50. https://doi.org/10.18799/24131830/2021/03/3100
Pyankov SV, Maximovich NG, Khayrulina EA, Berezina OA, Shikhov AN, Abdullin RK (2021) Monitoring acid mine drainage's effects on surface water in the Kizel Coal Basin with Sentinel-2 satellite images. Mine Water Environ. https://doi.org/10.1007/s10230-021-00761-7
Sahoo PK, Tripathy S, Panigrahi MK, Equeenuddin SM (2012) Mineralogy of Fe-precipitates and their role in metal retention from an acid mine drainage site in India. Mine Water Environ 31:344–352. https://doi.org/10.1007/s10230-012-0203-7
Santisteban M, Grande JA, de la Torre ML, Valente T, Perez-Ostale E, Garcia-Perez M (2016) Study of the transit and attenuation of pollutants in a water reservoir receiving acid mine drainage in the Iberian Pyrite Belt (SW Spain). Water Sci Technol Water Supply 16(1):128–134. https://doi.org/10.2166/ws.2015.122
Tarutis WJ, Unz RF (1995) Iron and manganese release in coal mine drainage wetland microcosms. Water Sci Technol 32(3):187–192. https://doi.org/10.2166/wst.1995.0140
Torre BM, Borrero-Santiago AR, Fabbri E, Guerra R (2019) Trace metal levels and toxicity in the Huelva Estuary (Spain): a case study with comparisons to historical levels from the past decades. Environ Chem Ecotoxicol 1:12–18. https://doi.org/10.1016/j.enceco.2019.07.002
Valente T, Grande JA, de la Torre ML, Santisteban M, Ceron JC (2013) Mineralogy and environmental relevance of AMD-precipitates from the Tharsis mines, Iberian Pyrite Belt (SW, Spain). Appl Geochem 39:11–25. https://doi.org/10.1016/j.apgeochem.2013.09.014
Valente T, Grande JA, de la Torre MR, Gomes P, Santisteban M, Borrego J, Sequeira Braga MA (2015) Mineralogy and geochemistry of a clogged mining reservoir affected by historical acid mine drainage in an abandoned mining area. J Geochem Explor 157:66–76. https://doi.org/10.1016/j.gexplo.2015.05.016
Wei X, Rodak CM, Zhang S, Han Y, Wolfe FA (2016) Mine drainage generation and control options. Water Environ Res 88(10):1409–1432. https://doi.org/10.2175/106143016X14696400495136
Wei X, Zhang S, Han Y, Wolfe FA (2017) Mine drainage: research and development. Water Environ Res 89(10):1384–1402. https://doi.org/10.2175/106143016X14696400495136
Zakrutkin VE, Gibkov EV, Reshetnyak OS, Reshetnyak VN (2020) River sediments as river waters' primary pollution indicator and secondary pollution source in east Donbass coal-mining areas. Bull Russ Acad Sci Geogr 84:259–271